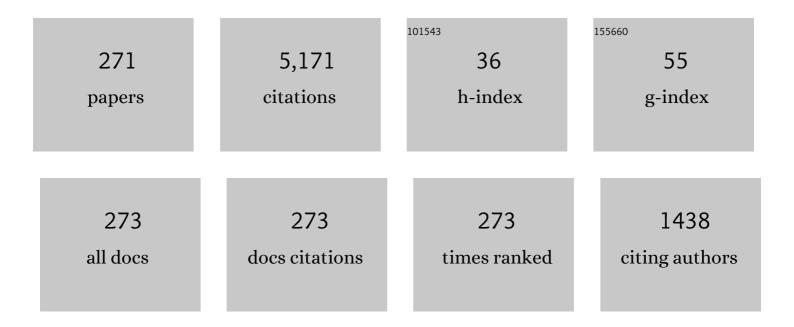
List of Publications by Year in descending order

Source: https://exaly.com/author-pdf/4280228/publications.pdf Version: 2024-02-01



#	Article	IF	CITATIONS
1	Electrical properties of poly-Ge on glass substrate grown by two-step solid-phase crystallization. Solid-State Electronics, 2009, 53, 1159-1164.	1.4	137
2	Investigation of grain boundaries in BaSi2 epitaxial films on Si(1 1 1) substrates using transmission electron microscopy and electron-beam-induced current technique. Journal of Crystal Growth, 2012, 348, 75-79.	1.5	133
3	Flux creep and irreversibility line in highâ€ŧemperature oxide superconductors. Applied Physics Letters, 1990, 56, 2039-2041.	3.3	120
4	Effect of amorphous Si capping layer on the hole transport properties of BaSi2 and improved conversion efficiency approaching 10% in p-BaSi2/n-Si solar cells. Applied Physics Letters, 2016, 109, .	3.3	109
5	Low-temperature (180 °C) formation of large-grained Ge (111) thin film on insulator using accelerated metal-induced crystallization. Applied Physics Letters, 2014, 104, .	3.3	96
6	High-Electrical-Conductivity Multilayer Graphene Formed by Layer Exchange with Controlled Thickness and Interlayer. Scientific Reports, 2019, 9, 4068.	3.3	89
7	Highly (111)-oriented Ge thin films on insulators formed by Al-induced crystallization. Applied Physics Letters, 2012, 101, 072106.	3.3	88
8	Giant Ge-on-Insulator Formation by Si–Ge Mixing-Triggered Liquid-Phase Epitaxy. Applied Physics Express, 0, 2, 045503.	2.4	87
9	Investigation of the recombination mechanism of excess carriers in undoped BaSi2 films on silicon. Journal of Applied Physics, 2012, 112, .	2.5	84
10	Multichannel taste sensor using electric potential changes in lipid membranes. Biosensors and Bioelectronics, 1994, 9, 359-364.	10.1	81
11	Influence of grain size and surface condition on minority-carrier lifetime in undoped <i>n</i> -BaSi2 on Si(111). Journal of Applied Physics, 2014, 115, .	2.5	80
12	Perpendicular magnetic anisotropy of Mn4N films on MgO(001) and SrTiO3(001) substrates. Journal of Applied Physics, 2014, 115, .	2.5	77
13	High-quality single-crystal Ge stripes on quartz substrate by rapid-melting-growth. Applied Physics Letters, 2009, 95, .	3.3	75
14	Determination of Bulk Minority-Carrier Lifetime in BaSi <sub>2</sub> Earth-Abundant Absorber Films by Utilizing a Drastic Enhancement of Carrier Lifetime by Post-Growth Annealing. Applied Physics Express, 2013, 6, 112302.	2.4	75
15	Temperature dependent metal-induced lateral crystallization of amorphous SiGe on insulating substrate. Applied Physics Letters, 2006, 89, 182120.	3.3	73
16	<i>In-situ</i> heavily <i>p</i> -type doping of over 1020 cmâ^3 in semiconducting BaSi2 thin films for solar cells applications. Applied Physics Letters, 2013, 102, .	3.3	72
17	High-hole mobility polycrystalline Ge on an insulator formed by controlling precursor atomic density for solid-phase crystallization. Scientific Reports, 2017, 7, 16981.	3.3	71
18	p-BaSi2/n-Si heterojunction solar cells with conversion efficiency reaching 9.0%. Applied Physics Letters, 2016, 108, .	3.3	69

#	Article	IF	CITATIONS
19	70 °C synthesis of high-Sn content (25%) GeSn on insulator by Sn-induced crystallization of amorphous Ge. Applied Physics Letters, 2015, 106, .	3.3	64
20	Molecular beam epitaxy of BaSi2 thin films on Si(001) substrates. Journal of Crystal Growth, 2012, 345, 16-21.	1.5	61
21	Ni-imprint induced solid-phase crystallization in Si1â^'xGex (x: 0–1) on insulator. Applied Physics Letters, 2007, 91, .	3.3	60
22	Current-voltage characteristics and self-sustained oscillations in dioleyl phosphate-millipore membranes. Biophysical Chemistry, 1984, 20, 39-59.	2.8	58
23	Impact of Ba to Si deposition rate ratios during molecular beam epitaxy on carrier concentration and spectral response of BaSi2 epitaxial films. Journal of Applied Physics, 2018, 123, 045703.	2.5	55
24	Improving carrier mobility of polycrystalline Ge by Sn doping. Scientific Reports, 2018, 8, 14832.	3.3	51
25	Improved photoresponsivity of semiconducting BaSi <sub>2</sub> epitaxial films grown on a tunnel junction for thin-film solar cells. Applied Physics Letters, 2012, 100, 152114.	3.3	50
26	Metal-induced layer exchange of group IV materials. Journal Physics D: Applied Physics, 2020, 53, 373002.	2.8	50
27	Analysis of the electrical properties of Cr/n-BaSi2 Schottky junction and n-BaSi2/p-Si heterojunction diodes for solar cell applications. Journal of Applied Physics, 2014, 115, .	2.5	49
28	Chip-size formation of high-mobility Ge strips on SiN films by cooling rate controlled rapid-melting growth. Applied Physics Letters, 2011, 99, 032103.	3.3	47
29	Operation of BaSi <sub>2</sub> homojunction solar cells on p <sup>+</sup> -Si(111) substrates and the effect of structure parameters on their performance. Applied Physics Express, 2019, 12, 041005.	2.4	47
30	Electrical characterization and conduction mechanism of impurity-doped BaSi2 films grown on Si(111) by molecular beam epitaxy. Thin Solid Films, 2012, 522, 95-99.	1.8	45
31	Fabrication and characterization of polycrystalline BaSi <sub>2</sub> by RF sputtering. Physica Status Solidi C: Current Topics in Solid State Physics, 2013, 10, 1759-1761.	0.8	45
32	Orientation Control of Large-Grained Si Films on Insulators by Thickness-Modulated Al-Induced Crystallization. Crystal Growth and Design, 2013, 13, 1767-1770.	3.0	44
33	p-BaSi2/n-Si heterojunction solar cells on Si(001) with conversion efficiency approaching 10%: comparison with Si(111). Applied Physics Express, 2018, 11, 062301.	2.4	42
34	On the oscillatory phenomenon in an oil/water interface. Biophysical Chemistry, 1985, 22, 151-158.	2.8	40
35	Selective formation of large-grained, (100)- or (111)-oriented Si on glass by Al-induced layer exchange. Journal of Applied Physics, 2014, 115, .	2.5	40
36	Influence of air exposure duration and a-Si capping layer thickness on the performance of p-BaSi2/n-Si heterojunction solar cells. AIP Advances, 2016, 6, .	1.3	40

#	Article	IF	CITATIONS
37	Sign of the spin-polarization in cobalt-iron nitride films determined by the anisotropic magnetoresistance effect. Journal of Applied Physics, 2014, 116, .	2.5	39
38	Relation of growth process to spatial patterns of electric potential and enzyme activity in bean roots. Biophysical Chemistry, 1987, 27, 39-58.	2.8	35
39	Epitaxial growth and magnetic characterization of ferromagnetic Co4N thin films on SrTiO3(001) substrates by molecular beam epitaxy. Journal of Crystal Growth, 2011, 336, 40-43.	1.5	35
40	Perpendicular magnetic anisotropy in Co <i>x</i> Mn4â^' <i>x</i> N ( <i>x</i> = 0 and 0.2) epitaxial films and possibility of tetragonal Mn4N phase. AIP Advances, 2016, 6, .	1.3	34
41	Low-Temperature (â^¼â€‰250°C) Cu-Induced Lateral Crystallization of Amorphous Ge on Insulator. Electrochemical and Solid-State Letters, 2011, 14, H274.	2.2	33
42	Stabilization effect of protons and divalent cations on membrane structures of lipids. Biophysical Chemistry, 1981, 14, 11-23.	2.8	32
43	Oscillations of electrical potential along a root of a higher plant. Biophysical Journal, 1990, 57, 269-279.	0.5	32
44	Formation of polycrystalline BaSi2 films by radio-frequency magnetron sputtering for thin-film solar cell applications. Thin Solid Films, 2013, 534, 116-119.	1.8	32
45	Precipitation control and activation enhancement in boron-doped p <i>+</i> -BaSi2 films grown by molecular beam epitaxy. Applied Physics Letters, 2014, 104, .	3.3	32
46	Evaluation of band offset at amorphous-Si/BaSi2 interfaces by hard x-ray photoelectron spectroscopy. Journal of Applied Physics, 2016, 119, .	2.5	32
47	Fabrication and characterization of BaSi <sub>2</sub> epitaxial films over 1 µm in thickness on Si(111). Japanese Journal of Applied Physics, 2014, 53, 04ER04.	1.5	31
48	Improved Surface Quality of the Metal-Induced Crystallized Ge Seed Layer and Its Influence on Subsequent Epitaxy. Crystal Growth and Design, 2015, 15, 1535-1539.	3.0	30
49	Simple way of finding Ba to Si deposition rate ratios for high photoresponsivity in BaSi <sub>2</sub> films by Raman spectroscopy. Applied Physics Express, 2019, 12, 055506.	2.4	30
50	Al-Induced oriented-crystallization of Si films on quartz and its application to epitaxial template for Ge growth. Solid-State Electronics, 2011, 60, 7-12.	1.4	29
51	Evaluation of potential variations around grain boundaries in BaSi2 epitaxial films by Kelvin probe force microscopy. Applied Physics Letters, 2013, 103, .	3.3	29
52	Polycrystalline thin-film transistors fabricated on high-mobility solid-phase-crystallized Ge on glass. Applied Physics Letters, 2019, 114, .	3.3	28
53	Negative spin polarization at the Fermi level in Fe4N epitaxial films by spin-resolved photoelectron spectroscopy. Journal of Applied Physics, 2012, 112, .	2.5	27
54	Millimeter-sized magnetic domains in perpendicularly magnetized ferrimagnetic Mn <sub>4</sub> N thin films grown on SrTiO <sub>3</sub> . Japanese Journal of Applied Physics, 2018, 57, 120310.	1.5	27

#	Article	IF	CITATIONS
55	Magnetic and magneto-transport properties of Mn4N thin films by Ni substitution and their possibility of magnetic compensation. Journal of Applied Physics, 2019, 125, .	2.5	27
56	Strong correlation between uniaxial magnetic anisotropic constant and in-plane tensile strain in Mn4N epitaxial films. AIP Advances, 2020, 10, .	1.3	27
57	N-type doping of BaSi2 epitaxial films by phosphorus ion implantation and thermal annealing. Thin Solid Films, 2014, 557, 90-93.	1.8	26
58	Direct synthesis of multilayer graphene on an insulator by Ni-induced layer exchange growth of amorphous carbon. Applied Physics Letters, 2017, 110, .	3.3	26
59	High-quality multilayer graphene on an insulator formed by diffusion controlled Ni-induced layer exchange. Applied Physics Letters, 2017, 111, .	3.3	26
60	Spectroscopic evidence of photogenerated carrier separation by built-in electric field in Sb-doped n-BaSi <sub>2</sub> /B-doped p-BaSi <sub>2</sub> homojunction diodes. Japanese Journal of Applied Physics, 2018, 57, 050310.	1.5	26
61	Thermoelectric Inorganic SiGe Film Synthesized on Flexible Plastic Substrate. ACS Applied Energy Materials, 0, , .	5.1	26
62	High hole mobility (≥500 cm <sup>2</sup> V <sup>â^'1</sup> s <sup>â^'1</sup> ) polycrystalline Ge films on GeO <sub>2</sub> -coated glass and plastic substrates. Applied Physics Express, 2019, 12, 015508.	2.4	25
63	Defect-free single-crystal Ge island arrays on insulator by rapid-melting-growth combined with seed-positioning technique. Applied Physics Letters, 2009, 95, 112107.	3.3	24
64	X-ray magnetic circular dichroism of ferromagnetic Co4N epitaxial films on SrTiO3(001) substrates grown by molecular beam epitaxy. Applied Physics Letters, 2011, 99, 252501.	3.3	23
65	Potential variations around grain boundaries in impurity-doped BaSi2 epitaxial films evaluated by Kelvin probe force microscopy. Journal of Applied Physics, 2014, 116, .	2.5	23
66	Control of grain size and crystallinity of poly-Si films on quartz by Al-induced crystallization. CrystEngComm, 2017, 19, 2305-2311.	2.6	23
67	Advanced solid-phase crystallization for high-hole mobility (450) Tj ETQq1 1 0.784314 rgBT /Overlock 10 Tf 50 26 2018, 11, 031302.	67 Td (cm 2.4	<sup>223</sup>
68	Metal Catalysts for Layer-Exchange Growth of Multilayer Graphene. ACS Applied Materials & Interfaces, 2018, 10, 41664-41669.	8.0	23
69	Magnetic reversal in rare-earth free Mn4 â^' <i>x</i> Ni <i>x</i> N epitaxial films below and above Ni composition needed for magnetic compensation around room temperature. Journal of Applied Physics, 2020, 127, .	2.5	23
70	Strain effects on polycrystalline germanium thin films. Scientific Reports, 2021, 11, 8333.	3.3	23
71	N-type doping of BaSi2 epitaxial films by arsenic ion implantation through a dose-dependent carrier generation mechanism. Thin Solid Films, 2014, 567, 105-108.	1.8	22
72	High-electron-mobility (370 cm2/Vs) polycrystalline Ge on an insulator formed by As-doped solid-phase crystallization. Scientific Reports, 2019, 9, 16558.	3.3	22

#	Article	IF	CITATIONS
73	High Quality Single-Crystalline Ge-Rich SiGe on Insulator Structures by Si-Doping Controlled Rapid Melting Growth. Applied Physics Express, 2010, 3, 031301.	2.4	21
74	Defect-free Ge-on-insulator with (100), (110), and (111) orientations by growth-direction-selected rapid-melting growth. Applied Physics Letters, 2010, 97, .	3.3	21
75	Single-crystalline (100) Ge networks on insulators by rapid-melting growth along hexagonal mesh-pattern. Applied Physics Letters, 2011, 98, .	3.3	21
76	Dependence of crystal orientation in Al-induced crystallized poly-Si layers on SiO2 insertion layer thickness. Journal of Crystal Growth, 2012, 356, 65-69.	1.5	21
77	Lattice and grain-boundary diffusions of boron atoms in BaSi2 epitaxial films on Si(111). Journal of Applied Physics, 2013, 113, .	2.5	21
78	Vertically Aligned Ge Nanowires on Flexible Plastic Films Synthesized by (111)-Oriented Ge Seeded Vapor–Liquid–Solid Growth. ACS Applied Materials & Interfaces, 2015, 7, 18120-18124.	8.0	21
79	Epitaxial growth and magnetic properties of Fe 4â^' x Mn x N thin films grown on MgO(0â€ <sup>-</sup> 0â€ <sup>-</sup> 1) substrates by molecular beam epitaxy. Journal of Crystal Growth, 2018, 489, 20-23.	1.5	21
80	Record-High Hole Mobility Germanium on Flexible Plastic with Controlled Interfacial Reaction. ACS Applied Electronic Materials, 2022, 4, 269-275.	4.3	21
81	Growth and electric current loops in plants. Biophysical Chemistry, 1989, 33, 161-176.	2.8	20
82	Indentation-induced low-temperature solid-phase crystallization of Si1â^'xGexâ€^(x=–1) on insulator. Applied Physics Letters, 2009, 94, .	3.3	20
83	Direct synthesis of highly textured Ge on flexible polyimide films by metal-induced crystallization. Applied Physics Letters, 2014, 104, .	3.3	20
84	Evaluation of minority carrier diffusion length of undoped n-BaSi <sub>2</sub> epitaxial thin films on Si(001) substrates by electron-beam-induced-current technique. Japanese Journal of Applied Physics, 2014, 53, 078004.	1.5	20
85	Measurement of valence-band offset at native oxide/BaSi2 interfaces by hard x-ray photoelectron spectroscopy. Journal of Applied Physics, 2016, 119, .	2.5	20
86	Significant photoresponsivity enhancement of polycrystalline BaSi <sub>2</sub> films formed on heated Si(111) substrates by sputtering. Applied Physics Express, 2018, 11, 071401.	2.4	20
87	Detection of local vibrational modes induced by intrinsic defects in undoped BaSi2 light absorber layers using Raman spectroscopy. Journal of Applied Physics, 2018, 124, 025301.	2.5	20
88	Marked enhancement of the photoresponsivity and minority-carrier lifetime of <mml:math xmlns:mml="http://www.w3.org/1998/Math/MathML"&gt; <mml:mrow> <mml:mi>BaS</mml:mi> <mml:msub> <mml mathvariant="normal"&gt;i <mml:mn>2 </mml:mn> </mml </mml:msub> </mml:mrow>  passivated with atomic hydrogen. Physical Review Materials, 2019, 3, .</mml:math 	:mi 2.4	20
89	(100) Orientation-Controlled Ge Giant-Stripes on Insulating Substrates by Rapid-Melting Growth Combined with Si Micro-Seed Technique. Applied Physics Express, 2010, 3, 075603.	2.4	19
00	X-ray magnetic circular dichroism for Co <sub><i>x</i></sub> Fe <sub>4â^'</sub> <sub><i>x</i></sub> N	9.5	10

 $(\langle i \rangle x \langle i \rangle \hat{a} \in \mathbb{M} = \hat{a} \in \mathbb{M} 0, 3, 4)$  films grown by molecular beam epitaxy. Journal of Applied Physics, 2014, 115, 17C712<sup>2.5</sup> 19

#	Article	IF	CITATIONS
91	Formation of BaSi2 heterojunction solar cells using transparent MoO <i>x</i> hole transport layers. Applied Physics Letters, 2015, 106, .	3.3	19
92	Effect of p-BaSi <sub>2</sub> layer thickness on the solar cell performance of p-BaSi <sub>2</sub> /n-Si heterojunction solar cells. Japanese Journal of Applied Physics, 2017, 56, 05DB03.	1.5	19
93	Low-Temperature (400 °C) Synthesis of Multilayer Graphene by Metal-Assisted Sputtering Deposition. ACS Omega, 2019, 4, 6677-6680.	3.5	19
94	Sb-doped crystallization of densified precursor for n-type polycrystalline Ge on an insulator with high carrier mobility. Applied Physics Letters, 2019, 114, .	3.3	19
95	350 °C synthesis of high-quality multilayer graphene on an insulator using Ni-induced layer exchange. Applied Physics Express, 2020, 13, 055502.	2.4	19
96	Molecular Beam Epitaxy of BaSi\$_{2}\$ Films with Grain Size over 4 \$mu\$m on Si(111). Japanese Journal of Applied Physics, 2012, 51, 098003.	1.5	18
97	Molecular beam epitaxy of boron doped p-type BaSi2 epitaxial films on Si(111) substrates for thin-film solar cells. Journal of Crystal Growth, 2013, 378, 201-204.	1.5	18
98	Local electronic states of Fe4N films revealed by x-ray absorption spectroscopy and x-ray magnetic circular dichroism. Journal of Applied Physics, 2015, 117, .	2.5	18
99	Low temperature synthesis of highly oriented p-type Si1- <i>x</i> Ge <i>x</i> ( <i>x</i> : 0–1) on an insulator by Al-induced layer exchange. Journal of Applied Physics, 2017, 122, .	2.5	18
100	Molecular beam epitaxy growth of Mn4â^'Ni N thin films on MgO(0 0 1) substrates and their magnetic properties. Journal of Crystal Growth, 2019, 507, 163-167.	1.5	18
101	<mml:math xmlns:mml="http://www.w3.org/1998/Math/MathML"><mml:mrow><mml:mi mathvariant="normal"&gt;C<mml:msub><mml:mi mathvariant="normal"&gt;o<mml:mi>x</mml:mi></mml:mi </mml:msub><mml:mi mathvariant="normal"&gt;M<mml:msub><mml:mi< td=""><td>3.2</td><td>18</td></mml:mi<></mml:msub></mml:mi </mml:mi </mml:mrow></mml:math>	3.2	18
102	Negative Anisotropic Magnetoresistance in γ'-Fe <sub>4</sub> N Epitaxial Films on <sup>a</sup> cmmtmi>xSrTiO <sub>3</sub> (001) Grown by Molecular Beam Epitaxy. Japanese Journal of Applied Physics, 2012, 51, 068001.	nml:mi>1.5	nml:mrow><, 17
103	Double-Layered Ge Thin Films on Insulators Formed by an Al-Induced Layer-Exchange Process. Crystal Growth and Design, 2013, 13, 3908-3912.	3.0	17
104	Large-Grained Polycrystalline (111) Ge Films on Insulators by Thickness-Controlled Al-Induced Crystallization. ECS Journal of Solid State Science and Technology, 2013, 2, Q195-Q199.	1.8	17
105	Orientation control of Ge thin films by underlayer-selected Al-induced crystallization. CrystEngComm, 2014, 16, 2578.	2.6	17
106	80 °C synthesis of thermoelectric nanocrystalline Ge film on flexible plastic substrate by Zn-induced layer exchange. Applied Physics Express, 2019, 12, 055501.	2.4	17
107	Magnetic compensation at two different composition ratios in rare-earth-free <mml:math xmlns:mml="http://www.w3.org/1998/Math/MathML"&gt;<mml:mrow><mml:msub><mml:mi>Mn</mml:mi><mml: mathvariant="normal"&gt;N</mml: </mml:msub></mml:mrow> ferrimagnetic films. Physical Review Materials. 2020. 4.</mml:math 	mrow> <m 2.4</m 	17   17   17   17   17   17   17   17
108	Temperature dependent Al-induced crystallization of amorphous Ge thin films on SiO2 substrates. Journal of Crystal Growth, 2013, 372, 189-192.	1.5	16

#	Article	IF	CITATIONS
109	Low-temperature crystallization of amorphous silicon and amorphous germanium by soft X-ray irradiation. Thin Solid Films, 2013, 534, 334-340.	1.8	16
110	Mechanism of strain relaxation in BaSi <sub>2</sub> epitaxial films on Si(111) substrates during postâ€growth annealing and application for film exfoliation. Physica Status Solidi C: Current Topics in Solid State Physics, 2013, 10, 1677-1680.	0.8	16
111	Photoresponse properties of undoped BaSi <sub>2</sub> epitaxial layers on n <sup>+</sup> -BaSi <sub>2</sub> /p <sup>+</sup> -Si(001) by molecular beam epitaxy. Japanese Journal of Applied Physics, 2014, 53, 058007.	1.5	16
112	Growth promotion of Al-induced crystallized Ge films on insulators by insertion of a Ge membrane below the Al layer. Thin Solid Films, 2014, 557, 143-146.	1.8	16
113	Epitaxial growth and magnetic properties of Ni <i>x</i> Fe4- <i>x</i> N ( <i>x</i> = 0, 1, 3, and 4) films on SrTiO3(001) substrates. Journal of Applied Physics, 2016, 120, .	2.5	16
114	Silver-induced layer exchange for polycrystalline germanium on a flexible plastic substrate. Journal of Applied Physics, 2017, 122, .	2.5	16
115	Three-step growth of highly photoresponsive BaSi2 light absorbing layers with uniform Ba to Si atomic ratios. Journal of Applied Physics, 2019, 126, .	2.5	16
116	Mesh-shape-and-size controlled rapid-melting growth for the formation of single-crystalline (100), (110), and (111) Ge networks on insulators. Applied Physics Letters, 2011, 98, .	3.3	15
117	Epitaxy of Orthorhombic BaSi\$_{2}\$ with Preferential In-Plane Crystal Orientation on Si(001): Effects of Vicinal Substrate and Annealing Temperature. Japanese Journal of Applied Physics, 2012, 51, 095501.	1.5	15
118	Structural study on phosphorus doping of BaSi2 epitaxial films by ion implantation. Thin Solid Films, 2013, 534, 470-473.	1.8	15
119	Fabrication and characterizations of phosphorusâ€doped nâ€type BaSi <sub>2</sub> epitaxial films grown by molecular beam epitaxy. Physica Status Solidi C: Current Topics in Solid State Physics, 2013, 10, 1753-1755.	0.8	15
120	Hard x-ray photoelectron spectroscopy study on valence band structure of semiconducting BaSi2. Journal of Applied Physics, 2013, 114, 123702.	2.5	15
121	Solid-phase crystallization of densified amorphous GeSn leading to high hole mobility (540 cm2/V s). Applied Physics Letters, 2019, 114, .	3.3	15
122	Orientation control of intermediate-composition SiGe on insulator by low-temperature Al-induced crystallization. Scripta Materialia, 2016, 122, 86-88.	5.2	14
123	Enhanced spectral response of semiconducting BaSi 2 films by oxygen incorporation. Thin Solid Films, 2017, 629, 17-21.	1.8	14
124	Molecular beam epitaxy of Co Fe4â^'N (0.4 <x<2.9) films="" journal="" of<br="" on="" srtio3(001)="" substrates.="" thin="">Crystal Growth, 2012, 357, 53-57.</x<2.9)>	1.5	13
125	Rotational and vibrational temperatures in a hydrogen discharge with a magnetic X-point. Physics of Plasmas, 2012, 19, 123503.	1.9	13
126	High-quality formation of multiply stacked SiGe-on-insulator structures by temperature-modulated successive rapid-melting-growth. Applied Physics Letters, 2013, 102, .	3.3	13

#	Article	IF	CITATIONS
127	High-hole mobility Si1-Ge (0.1 ≤ ≤) on an insulator formed by advanced solid-phase crystallization. Journal of Alloys and Compounds, 2018, 766, 417-420.	5.5	13
128	Investigation of defect levels in BaSi <sub>2</sub> epitaxial films by photoluminescence and the effect of atomic hydrogen passivation. Journal of Physics Communications, 2019, 3, 075005.	1.2	13
129	Zn-induced layer exchange of p- and n-type nanocrystalline SiGe layers for flexible thermoelectrics. Applied Physics Letters, 2020, 116, .	3.3	13
130	Atomic hydrogen passivation for photoresponsivity enhancement of boron-doped p-BaSi2 films and performance improvement of boron-doped p-BaSi2/n-Si heterojunction solar cells. Journal of Applied Physics, 2020, 127, .	2.5	13
131	Formation of high-photoresponsivity BaSi <sub>2</sub> films on glass substrate by radio-frequency sputtering for solar cell applications. Journal Physics D: Applied Physics, 2021, 54, 135106.	2.8	13
132	Investigation of electrically active defects in undoped BaSi2 light absorber layers using deep-level transient spectroscopy. Japanese Journal of Applied Physics, 2018, 57, 075801.	1.5	12
133	Perpendicular magnetic anisotropy in ferrimagnetic Mn4N films grown on (LaAlO3)0.3(Sr2TaAlO6)0.7(0Â0Â1) substrates by molecular beam epitaxy. Journal of Crystal Growth, 2020, 535, 125566.	1.5	12
134	Structural Study of BF <sub>2</sub> Ion Implantation and Post Annealing of BaSi <sub>2</sub> Epitaxial Films. Japanese Journal of Applied Physics, 2011, 50, 121202.	1.5	11
135	Electronic structures and magnetic moments of Co3FeN thin films grown by molecular beam epitaxy. Applied Physics Letters, 2013, 103, .	3.3	11
136	Characterization of defect levels in undoped n-BaSi <sub>2</sub> epitaxial films on Si(111) by deep-level transient spectroscopy. Japanese Journal of Applied Physics, 2015, 54, 07JE01.	1.5	11
137	Reduction in interface defect density in p-BaSi <sub>2</sub> /n-Si heterojunction solar cells by a modified pretreatment of the Si substrate. Japanese Journal of Applied Physics, 2018, 57, 025501.	1.5	11
138	Impact of deposition pressure and two-step growth technique on the photoresponsivity enhancement of polycrystalline BaSi <sub>2</sub> films formed by sputtering. Applied Physics Express, 2019, 12, 021004.	2.4	11
139	Spontaneous formation of the spatial pattern of electric potential in biological systems. Ferroelectrics, 1988, 86, 269-279.	0.6	10
140	Self-organization of Ge(111)/Al/glass structures through layer exchange in metal-induced crystallization. CrystEngComm, 2014, 16, 9590-9595.	2.6	10
141	Influence of Substrate on Crystal Orientation of Large-Grained Si Thin Films Formed by Metal-Induced Crystallization. International Journal of Photoenergy, 2015, 2015, 1-7.	2.5	10
142	Growth and magnetic properties of epitaxial Fe4N films on insulators possessing lattice spacing close to Si(001) plane. Journal of Crystal Growth, 2016, 455, 66-70.	1.5	10
143	Multilayer graphene on insulator formed by Co-induced layer exchange. Japanese Journal of Applied Physics, 2017, 56, 05DE03.	1.5	10
144	Improving the photoresponse spectra of BaSi2 layers by capping with hydrogenated amorphous Si layers prepared by radio-frequency hydrogen plasma. AIP Advances, 2018, 8, 055306.	1.3	10

#	Article	IF	CITATIONS
145	High photoresponsivity in a GaAs film synthesized on glass using a pseudo-single-crystal Ge seed layer. Applied Physics Letters, 2019, 114, .	3.3	10
146	Multilayer Graphene Battery Anodes on Plastic Sheets for Flexible Electronics. ACS Applied Energy Materials, 2020, 3, 8410-8414.	5.1	10
147	Thickness-dependent thermoelectric properties of Si1â^' <i>x</i> Ge <i>x</i> films formed by Al-induced layer exchange. Journal of Applied Physics, 2021, 129, .	2.5	10
148	High thermoelectric power factors in polycrystalline germanium thin films. Applied Physics Letters, 2021, 119, .	3.3	10
149	Zn <sub>1–<i>x</i></sub> Ge <sub><i>x</i></sub> O <sub><i>y</i></sub> Passivating Interlayers for BaSi <sub>2</sub> Thin-Film Solar Cells. ACS Applied Materials & Interfaces, 2022, 14, 13828-13835.	8.0	10
150	Dynamic property of membrane formation in a protoplasmic droplet of nitella. Biophysical Chemistry, 1985, 21, 295-313.	2.8	9
151	Lattice and grain-boundary diffusions of impurity atoms in BaSi2 epitaxial layers grown by molecular beam epitaxy. Journal of Crystal Growth, 2013, 378, 189-192.	1.5	9
152	Diffusion coefficients of impurity atoms in BaSi2epitaxial films grown by molecular beam epitaxy. Japanese Journal of Applied Physics, 2014, 53, 04ER02.	1.5	9
153	Effects of flexible substrate thickness on Al-induced crystallization of amorphous Ge thin films. Thin Solid Films, 2015, 583, 221-225.	1.8	9
154	Boron-doped p-BaSi2/n-Si solar cells formed on textured n-Si(0 0 1) with a pyramid structure consisting of {1 1 1} facets. Journal of Crystal Growth, 2017, 475, 186-191.	1.5	9
155	Thin-film thermoelectric generator based on polycrystalline SiGe formed by Ag-induced layer exchange. Applied Physics Letters, 2020, 117, .	3.3	9
156	Solar cell operation of sputter-deposited n-BaSi <sub>2</sub> /p-Si heterojunction diodes and characterization of defects by deep-level transient spectroscopy. Applied Physics Express, 2021, 14, 051010.	2.4	9
157	Negative Anisotropic Magnetoresistance in γ'-Fe <sub>4</sub> N Epitaxial Films on SrTiO <sub>3</sub> (001) Grown by Molecular Beam Epitaxy. Japanese Journal of Applied Physics, 2012, 51, 068001.	1.5	9
158	Nucleation-Controlled Metal-Induced Lateral Crystallization of Amorphous Si1-xGexwith Whole Ge Fraction on Insulator. Japanese Journal of Applied Physics, 2008, 47, 1876-1879.	1.5	8
159	Potential variation around grain boundaries in BaSi2 films grown on multicrystalline silicon evaluated using Kelvin probe force microscopy. Journal of Applied Physics, 2014, 116, .	2.5	8
160	Effect of BaSi <sub>2</sub> template growth duration on the generation of defects and performance of p-BaSi <sub>2</sub> /n-Si heterojunction solar cells. Japanese Journal of Applied Physics, 2018, 57, 042301.	1.5	8
161	Investigation of native defects in BaSi <sub>2</sub> epitaxial films by electron paramagnetic resonance. Applied Physics Express, 2019, 12, 061005.	2.4	8
162	Significant enhancement of photoresponsivity in As-doped n-BaSi <sub>2</sub> epitaxial films by atomic hydrogen passivation. Applied Physics Express, 2020, 13, 051001.	2.4	8

#	Article	IF	CITATIONS
163	Improved thermoelectric performance of flexible p-type SiGe films by B-doped Al-induced layer exchange. Journal Physics D: Applied Physics, 2020, 53, 075105.	2.8	8
164	Mechanisms of carrier lifetime enhancement and conductivity-type switching on hydrogen-incorporated arsenic-doped BaSi2. Thin Solid Films, 2021, 724, 138629.	1.8	8
165	Layer exchange synthesis of multilayer graphene. Nanotechnology, 2021, 32, 472005.	2.6	8
166	Effect of post-annealing on the significant photoresponsivity enhancement of BaSi <sub>2</sub> epitaxial films on Si(111). Applied Physics Express, 2021, 14, 021003.	2.4	8
167	Impact of radio-frequency power on the photoresponsivity enhancement of BaSi <sub>2</sub> films formed by sputtering. Applied Physics Express, 2020, 13, 085511.	2.4	8
168	Sn Concentration Effects on Polycrystalline GeSn Thin Film Transistors. IEEE Electron Device Letters, 2021, 42, 1735-1738.	3.9	8
169	Al-induced crystallization of amorphous Ge thin films on conducting layer coated glass substrates. Japanese Journal of Applied Physics, 2014, 53, 04EH01.	1.5	7
170	Structural characterization of polycrystalline Ge thin films on insulators formed by diffusion-enhanced Al-induced layer exchange. Japanese Journal of Applied Physics, 2014, 53, 04EH03.	1.5	7
171	Large-grained (111)-oriented Si/Al/SiO2 structures formed by diffusion-controlled Al-induced layer exchange. Thin Solid Films, 2014, 557, 147-150.	1.8	7
172	Mössbauer study on epitaxial Co <i>x</i> Fe4â^' <i>x</i> N films grown by molecular beam epitaxy. Journal of Applied Physics, 2015, 117, .	2.5	7
173	Effects of Al grain size on metal-induced layer exchange growth of amorphous Ge thin film on glass substrate. Thin Solid Films, 2017, 626, 190-193.	1.8	7
174	Minority-carrier lifetime and photoresponse properties of B-doped p-BaSi <sub>2</sub> , a potential light absorber for solar cells. Japanese Journal of Applied Physics, 2017, 56, 05DB01.	1.5	7
175	Growth of BaSi2 continuous films on Ge(111) by molecular beam epitaxy and fabrication of p-BaSi2/n-Ge heterojunction solar cells. Japanese Journal of Applied Physics, 2017, 56, 05DB02.	1.5	7
176	Impact of Amorphous-C/Ni Multilayers on Ni-Induced Layer Exchange for Multilayer Graphene on Insulators. ACS Omega, 2019, 4, 14251-14254.	3.5	7
177	Correlation of native defects between epitaxial films and polycrystalline BaSi <sub>2</sub> bulks based on photoluminescence spectra. Applied Physics Express, 2019, 12, 111001.	2.4	7
178	Modeling the effects of defect parameters on the performance of a p-BaSi2/n-Si heterojunction solar cell. Solar Energy Materials and Solar Cells, 2020, 205, 110244.	6.2	7
179	Influence of Ba-to-Si deposition rate ratios on the electrical and optical properties of B-doped BaSi2 epitaxial films. Japanese Journal of Applied Physics, 2020, 59, SFFA04.	1.5	7
180	Fabrication of As-doped n-type BaSi2 epitaxial films grown by molecular beam epitaxy. Japanese Journal of Applied Physics, 2020, 59, SFFA01.	1.5	7

#	Article	IF	CITATIONS
181	High-temperature post-annealing effect on the surface morphology and photoresponse and electrical properties of B-doped BaSi2 films grown by molecular beam epitaxy under various Ba-to-Si deposition rate ratios. Journal of Crystal Growth, 2022, 578, 126429.	1.5	7
182	High electron mobility in randomly oriented polycrystalline BaSi <sub>2</sub> films formed through radio-frequency sputtering. AIP Advances, 2022, 12, 045120.	1.3	7
183	Electrical characteristics in an excitable element of lipid membrane. Biophysical Chemistry, 1991, 41, 143-156.	2.8	6
184	Transfer-free synthesis of highly ordered Ge nanowire arrays on glass substrates. Applied Physics Letters, 2015, 107, 133102.	3.3	6
185	Control of electrical properties of BaSi2 thin films by alkali-metal doping using alkali-metal fluorides. Thin Solid Films, 2016, 603, 218-223.	1.8	6
186	Fe-induced layer exchange of multilayer graphene for rechargeable battery anodes. Applied Physics Express, 2020, 13, 025501.	2.4	6
187	Drastic enhancement of photoresponsivity in C-doped BaSi2 films formed by radio-frequency sputtering. Japanese Journal of Applied Physics, 2020, 59, SFFA06.	1.5	6
188	Growth conditions for high-photoresponsivity randomly oriented polycrystalline BaSi <sub>2</sub> films by radio-frequency sputtering: Comparison with BaSi <sub>2</sub> epitaxial films. Applied Physics Express, 2022, 15, 025502.	2.4	6
189	Flexible Thermoelectric Generator Based on Polycrystalline SiGe Thin Films. Materials, 2022, 15, 608.	2.9	6
190	Theory of electric dissipative structure in Characean internode. Biophysical Chemistry, 1987, 27, 149-172.	2.8	5
191	High-Hole-Mobility Single-Crystalline Ge Thin Films Formed on Insulating Substrates by SiGe Mixing-Triggered Directional Melting Growth. Japanese Journal of Applied Physics, 2010, 49, 04DA08.	1.5	5
192	SiGe-Mixing-Triggered Rapid-Melting-Growth of High-Mobility Ge-On-Insulator. Key Engineering Materials, 2011, 470, 8-13.	0.4	5
193	Nano-lithography free formation of high density Ge-on-insulator network for epitaxial template. Applied Physics Letters, 2012, 100, 092111.	3.3	5
194	Formation of large-grain-sized BaSi2 epitaxial layers grown on Si(111) by molecular beam epitaxy. Journal of Crystal Growth, 2013, 378, 193-197.	1.5	5
195	Epitaxial growth of ferromagnetic CoxFe4â~'xN thin films on SrTiO3 (001) and magneticproperties. Journal of Crystal Growth, 2013, 378, 342-346.	1.5	5
196	Cross-sectional potential profile across a BaSi2pn junction by Kelvin probe force microscopy. Japanese Journal of Applied Physics, 2015, 54, 030306.	1.5	5
197	Effect of interlayer on silver-induced layer exchange crystallization of amorphous germanium thin film on insulator. Japanese Journal of Applied Physics, 2017, 56, 05DE04.	1.5	5
198	Effects of boron and hydrogen doping on the enhancement of photoresponsivity and photoluminescence of BaSi <sub>2</sub> epitaxial films. Japanese Journal of Applied Physics, 2020, 59, SFFA08.	1.5	5

#	Article	IF	CITATIONS
199	Comparison of C doping technique between SiC and C targets for high-photoresponsivity BaSi <sub>2</sub> films by radio-frequency sputtering. Japanese Journal of Applied Physics, 2021, 60, 058001.	1.5	5
200	Composition dependent properties of p- and n-type polycrystalline group-IV alloy thin films. Journal of Alloys and Compounds, 2021, 887, 161306.	5.5	5
201	Formation of single-crystalline Ge stripes on quartz substrates by SiGe mixing-triggered liquid-phase epitaxy. Thin Solid Films, 2010, 518, S179-S181.	1.8	4
202	Large photoresponsivity in semiconducting BaSi2 epitaxial films grown on Si(001) substrates by molecular beam epitaxy. Journal of Crystal Growth, 2013, 378, 198-200.	1.5	4
203	Highly oriented epitaxial (α′′+α′)-Fe16N2 films on α-Fe(001) buffered MgAl2O4(001) substrates and the magnetization. Journal of Crystal Growth, 2017, 468, 691-695.	<sup>2ir</sup> 1.5	4
204	Structural characterization and magnetic properties of L10-MnAl films grown on different underlayers by molecular beam epitaxy. Journal of Crystal Growth, 2018, 486, 19-23.	1.5	4
205	Solid-phase crystallization of gallium arsenide thin films on insulators. Materials Science in Semiconductor Processing, 2021, 124, 105623.	4.0	4
206	Effects of Ba-to-Si deposition rate ratios on the electrical and photoresponse properties of arsenic-doped n-type BaSi2 films. Thin Solid Films, 2021, 738, 138969.	1.8	4
207	Electronic sensing of the taste of beer and other foodstuffs. , 0, , .		3
208	Evaluation of diffusion coefficients of <i>n</i> â€ŧype impurities in MBEâ€grown BaSi <sub>2</sub> epitaxial layers. Physica Status Solidi C: Current Topics in Solid State Physics, 2013, 10, 1762-1764.	0.8	3
209	Fabrication of L-shaped Fe4N ferromagnetic narrow wires and position control of magnetic domain wall with magnetic field. Japanese Journal of Applied Physics, 2015, 54, 028003.	1.5	3
210	Decrease in electrical contact resistance of Sb-doped n <sup>+</sup> -BaSi <sub>2</sub> layers and spectral response of an Sb-doped n <sup>+</sup> -BaSi <sub>2</sub> /undoped BaSi <sub>2</sub> structure for solar cells. Japanese Journal of Applied Physics, 2018, 57, 031202.	1.5	3
211	Minority carrier lifetime of Ge film epitaxial grown on a large-grain seed layer on glass. Thin Solid Films, 2019, 681, 98-102.	1.8	3
212	Influence of grain boundaries on the properties of polycrystalline germanium. Journal of Applied Physics, 2020, 128, .	2.5	3
213	Improving photoresponsivity in GaAs film grown on Al-induced-crystallized Ge on an insulator. AIP Advances, 2020, 10, 015153.	1.3	3
214	Fabrication of high-photoresponsivity BaSi <sub>2</sub> films formed on conductive layers by radio-frequency sputtering. Applied Physics Express, 2020, 13, 075506.	2.4	3
215	Effects of molecular beam epitaxy growth conditions on grain size and lattice strain in <i>a</i> -axis-oriented BaSi <sub>2</sub> films. Japanese Journal of Applied Physics, 2020, 59, SFFA09.	1.5	3
216	Solidâ€phase crystallization of GeSn thin films on GeO 2 â€coated glass. Physica Status Solidi - Rapid Research Letters, 0, , 2100509.	2.4	3

#	Article	IF	CITATIONS
217	Three-Dimensionally Orientation-Controlled Ge Rods on an Insulator Formed by Low-Temperature Ni-Induced Lateral Crystallization. Crystal Growth and Design, 2022, 22, 1123-1129.	3.0	3
218	Machine learning of fake micrographs for automated analysis of crystal growth process. Science and Technology of Advanced Materials Methods, 2022, 2, 213-221.	1.3	3
219	Low-temperature solid-phase crystallization of amorphous SiGe films on glass by imprint technique. Solid-State Electronics, 2008, 52, 1221-1224.	1.4	2
220	Position-Controlled Growth of SiGe Crystal Grains on Insulator by Indentation-Induced Solid-Phase Crystallization. Japanese Journal of Applied Physics, 2009, 48, 03B007.	1.5	2
221	Growth-Direction Dependent Rapid-Melting-Growth of Ge-On-Insulator (GOI) and its Application to Ge Mesh-Growth. ECS Transactions, 2011, 35, 55-60.	0.5	2
222	Growth-direction-dependent characteristics of Ge-on-insulator by Si–Ge mixing triggered melting growth. Solid-State Electronics, 2011, 60, 18-21.	1.4	2
223	Realization of Large-Domain Barium Disilicide Epitaxial Thin Film by Introduction of Miscut to Si(111) Substrate. Japanese Journal of Applied Physics, 2012, 51, 10NB06.	1.5	2
224	Effect of atomic-hydrogen irradiation on reduction of residual carrier concentration in β-FeSi2 films grown on Si substrates by atomic-hydrogen-assisted molecular beam epitaxy. Journal of Crystal Growth, 2013, 378, 365-367.	1.5	2
225	Grain size dependent photoresponsivity in GaAs films formed on glass with Ge seed layers. Scientific Reports, 2021, 11, 10159.	3.3	2
226	Four-step heating process for solid-phase crystallization of Ge leading to high carrier mobility. Applied Physics Express, 2020, 13, 101005.	2.4	2
227	Epitaxy of Orthorhombic BaSi2with Preferential In-Plane Crystal Orientation on Si(001): Effects of Vicinal Substrate and Annealing Temperature. Japanese Journal of Applied Physics, 2012, 51, 095501.	1.5	2
228	Structural Study of BF2Ion Implantation and Post Annealing of BaSi2Epitaxial Films. Japanese Journal of Applied Physics, 2011, 50, 121202.	1.5	2
229	Molecular Beam Epitaxy of BaSi2Films with Grain Size over 4 µm on Si(111). Japanese Journal of Applied Physics, 2012, 51, 098003.	1.5	2
230	Strained single-crystal GOI (Ge on Insulator) arrays by rapid-melting growth from Si (111) micro-seeds. Solid-State Electronics, 2011, 60, 22-25.	1.4	1
231	Effect of Solid-Phase-Epitaxy Si Layers on Suppression of Sb Diffusion from Sb-Doped n <sup>+</sup> -BaSi <sub>2</sub> /p <sup>+</sup> -Si Tunnel Junction to Undoped BaSi <sub>2</sub> Overlayers. Japanese Journal of Applied Physics, 2012, 51, 04DP01.	1.5	1
232	Atomically-Coherent-Coalescence of Two Growth-Fronts in Ge Stripes on Insulator by Rapid-Melting Lateral-Crystallization. ECS Journal of Solid State Science and Technology, 2013, 2, P54-P57.	1.8	1
233	Investigation of the tunneling properties and surface morphologies of BaSi2 /Si tunnel junctions for BaSi2 solar cell applications. Physica Status Solidi C: Current Topics in Solid State Physics, 2013, 10, 1765-1768.	0.8	1
234	Fabrication of BaSi2 films on (111)-oriented Si layers formed by inverted Al-induced crystallization method on glass structure. Physica Status Solidi C: Current Topics in Solid State Physics, 2013, 10, 1769-1772.	0.8	1

#	Article	IF	CITATIONS
235	Epitaxial growth of BaSi2films with large grains using vicinal Si(111) substrates. Physica Status Solidi C: Current Topics in Solid State Physics, 2013, 10, 1756-1758.	0.8	1
236	Coherent lateral-growth of Ge over insulating film by rapid-melting-crystallization. Thin Solid Films, 2014, 557, 135-138.	1.8	1
237	Cross-sectional electric field distributions in BaSi2 homo and BaSi2/Si hetero pn junctions. , 2015, , .		1
238	Fabrication and characterization of BaSi2 films on Ge(111) substrates by molecular beam epitaxy. , 2015, , $\cdot$		1
239	Effect of Diffusion Control Layer on Reverse Al-Induced Layer Exchange Process for High-Quality Ge/Al/Class Structure. Journal of Electronic Materials, 2015, 44, 1377-1381.	2.2	1
240	Electrical detection of magnetic domain wall in Fe4N nanostrip by negative anisotropic magnetoresistance effect. Journal of Applied Physics, 2016, 120, .	2.5	1
241	Sn-inserted Al-induced layer exchange for large-grained GeSn thin films on insulator. Thin Solid Films, 2016, 616, 316-319.	1.8	1
242	Fabrication of SrGe2 thin films on Ge (100), (110), and (111) substrates. Nanoscale Research Letters, 2018, 13, 22.	5.7	1
243	Impact of the carbon membrane inserted below Ni in the layer exchange of multilayer graphene. CrystEngComm, 2020, 22, 3106-3109.	2.6	1
244	Effect of Solid-Phase-Epitaxy Si Layers on Suppression of Sb Diffusion from Sb-Doped n <sup>+</sup> -BaSi <sub>2</sub> /p <sup>+</sup> -Si Tunnel Junction to Undoped BaSi <sub>2</sub> Overlayers. Japanese Journal of Applied Physics, 2012, 51, 04DP01.	1.5	1
245	Formation of SiGe Quasi-Single Crystal Grain on Insulator by Indentation-Induced Solid-Phase Crystallization. ECS Transactions, 2009, 16, 219-222.	0.5	0
246	Liquid-phase epitaxial growth of Ge island on insulator using Ni-imprint-induced Si crystal as seed. Thin Solid Films, 2010, 518, S182-S185.	1.8	0
247	High-mobility defect-free ge single-crystals by rapid melting growth on insulating substrates. , 2010, , .		0
248	Crystallization mechanism of thick a-Si <inf>0.5</inf> Ge <inf>0.5</inf> film by excimer laser annealing. , 2012, , .		0
249	Improved internal quantum efficiency in high-quality BaSi <inf>2</inf> films grown by molecular beam epitaxy. , 2012, , .		0
250	Investigation of the carrier recombination process in undoped barium disilicide epitaxial films. , 2012, ,		0
251	Characterization of grain boundary properties in BaSi2 epitaxial films on Si(111) and Si(001) by Kelvin probe force microscopy. , 2013, , .		0
252	Improvement of excess-carrier lifetime in BaSi <inf>2</inf> epitaxial films by post-growth annealing. , 2013, , .		0

#	Article	IF	CITATIONS
253	(Invited) Hybrid-Formation of Ge-on-Insulator Structures on Si Platform by SiGe-Mixing-Triggered Rapid-Melting Growth A Road to Artificial Crystal ECS Transactions, 2013, 50, 59-70.	0.5	0
254	Enhanced p-type conductivity and band gap narrowing in heavily B-doped p-BaSi <inf>2</inf> films grown by molecular beam epitaxy. , 2013, , .		0
255	Effect of Ge/Al thickness on Al-induced crystallization of amorphous Ge layers on glass substrates. Physica Status Solidi C: Current Topics in Solid State Physics, 2013, 10, 1781-1784.	0.8	Ο
256	Fabrication of n <sup>+</sup> â€BaSi <sub>2</sub> /p <sup>+</sup> â€Si tunnel junction on Si(001) surface for characterization of photoresponse properties of BaSi <sub>2</sub> epitaxial films. Physica Status Solidi C: Current Topics in Solid State Physics, 2013, 10, 1773-1776.	0.8	0
257	Electrical and optical characterizations of an n-BaSi <inf>2</inf> /p-Si hetero-junction for solar cell applications. , 2014, , .		Ο
258	Grain boundaries characterization of semiconducting BaSi <inf>2</inf> thin films on a polycrystalline Si substrate. , 2014, , .		0
259	Engineering of p-n junction for high efficiency semiconducting BaSi2 based thin film solar cells. , 2014, , .		Ο
260	Si-based new material for high-efficiency thin film solar cells. , 2014, , .		0
261	Control of domain wall position in L-shaped Fe <inf>4</inf> N negatively spin polarized ferromagnetic nanowire. , 2015, , .		Ο
262	Band alignments at native oxide/BaSi <inf>2</inf> and amorphous-Si/BaSi <inf>2</inf> interfaces measured by hard x-ray photoelectron spectroscopy. , 2016, , .		0
263	Fabrication and characterizations of nitrogen-doped BaSi2 epitaxial films grown by molecular beam epitaxy. Journal of Crystal Growth, 2017, 471, 37-41.	1.5	0
264	Demonstration of BaSi <inf>2</inf> pn homojunction solar cells and improvement of photoresponsivity of BaSi <inf>2</inf> absorbers by Ba/Si deposition rate ratio. , 2018, , .		0
265	Photoresponsivity improvement of BaSi <inf>2</inf> epitaxial films by capping with hydrogenated amorphous Si layers by radio-frequency <inf>2</inf> plasma. , 2018, , .		Ο
266	Deep level transient spectroscopy characterization of BaSi <inf>2</inf> light absorbers. , 2018, , .		0
267	Investigation of p-BaSi <inf>2</inf> /n-Si heterojunction solar cells on Si(001) and comparison to those on Si(111). , 2018, , .		Ο
268	Expansion of Solid-phase Interactions between Carbon and Metals: Layer Exchange for Multilayer Graphene on Insulator. , 2019, , .		0
269	Significant improvement on electrical properties of BaSi2 due to atomic H passivation by radio-frequency plasma. , 2019, , .		0
270	Effects of sputtering pressure and temperature of ITO electrodes on the performance of p-BaSi <sub>2</sub> /n-Si heterojunction solar cells. Japanese Journal of Applied Physics, 2020, 59, SFFA07.	1.5	0

# A	Article	IF	CITATIONS
271 L	Low-temperature solid-phase crystallization of group IV material thin films. , 2021, , .		0